

# Linear stability of magnetohydrodynamic flow in a perfectly conducting rectangular duct

By JĀNIS PRIEDE, SVETLANA ALEKSANDROVA  
and SERGEI MOLOKOV

(Received 12 June 2012)

We analyse numerically the linear stability of a liquid metal flow in a rectangular duct with perfectly electrically conducting walls subject to a uniform transverse magnetic field. A non-standard three dimensional vector stream function/vorticity formulation is used with Chebyshev collocation method to solve the eigenvalue problem for small-amplitude perturbations. A relatively weak magnetic field is found to render the flow linearly unstable as two weak jets appear close to the centre of the duct at the Hartmann number  $Ha \approx 9.6$ . In a sufficiently strong magnetic field, the instability following the jets becomes confined in the layers of characteristic thickness  $\delta \sim Ha^{-1/2}$  located at the walls parallel to the magnetic field. In this case the instability is determined by  $\delta$ , which results in both the critical Reynolds and wavenumbers numbers scaling as  $\sim \delta^{-1}$ . Instability modes can have one of the four different symmetry combinations along and across the magnetic field. The most unstable is a pair of modes with an even distribution of vorticity along the magnetic field. These two modes represent strongly non-uniform vortices aligned with the magnetic field, which rotate either in the same or opposite senses across the magnetic field. The former enhance while the latter weaken one another provided that the magnetic field is not too strong or the walls parallel to the field are not too far apart. In a strong magnetic field, when the vortices at the opposite walls are well separated by the core flow, the critical Reynolds and wavenumbers for both of these instability modes are the same:  $Re_c \approx 642Ha^{1/2} + 8.9 \times 10^3 Ha^{-1/2}$  and  $k_c \approx 0.477Ha^{1/2}$ . The other pair of modes, which differs from the previous one by an odd distribution of vorticity along the magnetic field, is more stable with approximately four times higher critical Reynolds number.

---

## 1. Introduction

Understanding instabilities in magnetohydrodynamic (MHD) flows in ducts is of great importance for liquid metal flows in blankets for fusion reactors (Bühler 2007). Blankets consist of rectangular ducts in which the liquid metal flows in a high, transverse magnetic field of between 5 and 10 T. The aim of these devices is to cool plasma chamber and to breed and to remove tritium. This can be assisted by mixing of the flow by turbulence if it can be sustained in the presence of a magnetic field. A high magnetic field is known to damp turbulence by means of the Lorentz force. At the same time, the magnetic field can also affect the base velocity profile in such a way as to create inflection lines (Kakutani 1964) and even jets (Hunt 1965) thus making the flow more unstable. These two competing effects balancing each other on a certain length scale result in relatively simple asymptotics for the instability threshold. The most dangerous perturbations are usually associated with the largest length scale on which the magnetic damping becomes comparable with the viscous one. This happens in the so-called parallel layers with the relative

thickness  $\sim Ha^{-1/2}$  (Braginskii 1960). Linear stability of these layers for a duct with insulating walls (Shercliff 1953) has been considered in a quasi-two-dimensional approximation by Poth  rat (2007), who found the critical Reynolds number  $Re_c \approx 4.8 \times 10^4 Ha^{1/2}$ . It is an extremely high, however, typical value for the linear stability of exponential velocity profiles, which have the critical Reynolds number around fifty thousand based on the boundary layer thickness (Drazin & Reid 1981). This high threshold is of little practical relevance because the instability for exponential velocity profile is known to be subcritical (Hocking 1975). This is the case also for the stability of Hartmann layer (Lock 1955), which is subcritical too (Lifshits & Shtern 1979; Moresco & Alboussiere 2003) with the experimentally found Reynolds number for the onset of turbulence in straight and annular ducts of rectangular cross-sections being respectively around  $225 Ha$  (Murgatroyd 1953; Brouillette & Lykoudis 1967) and  $380 Ha$  (Moresco & Alboussiere 2004). Marginal turbulent flow states have been observed by Shatrov & Gerbeth (2010) significantly below the linear stability threshold in numerical simulations of insulating duct flow subject to a transverse magnetic field of moderate strength.

The stability of MHD flows strongly varies with the electrical conductivity of the duct walls. For example, Hunt’s flow, which develops in a rectangular duct when the walls perpendicular to the magnetic field are perfectly conducting while the parallel ones are insulating, has a relatively low linear stability threshold  $Re_c \approx 91 Ha^{1/2}$  and  $\bar{Re}_c \approx 112$  based on the maximum and average velocities, respectively (Priede, Aleksandrova & Molokov 2010). The low stability of Hunt’s flow is due to two strong jets, which develop in a sufficiently strong magnetic field along the insulating walls and attain a velocity  $\sim Ha$  relative to that of the core flow (Hunt 1965). Although the relative velocity of jets reduces as  $\sim Ha^{1/2}/c$  with the increase of the wall conductance ratio  $c \gtrsim Ha^{-1/2}$  (Walker 1981), weak jets with the relative velocity  $O(1)$  still persist at the parallel walls also in the limit of perfectly conducting duct (Uflyand 1961; Chang & Lundgren 1961). The presence of jets with inherent inflection points suggests that this flow may also be highly unstable similar to Hunt’s flow. It is the aim of the present study to investigate linear stability of this flow, which is the last basic MHD duct flow configuration whose linear stability may be not only of theoretical but also of experimental relevance. We first investigate the case of square duct and find the high-field asymptotics of the instability threshold which are then generalized to arbitrary aspect ratios.

The paper is organised as follows. The problem is formulated in §2 below. In §3 we present and discuss numerical results for a square duct in a vertical magnetic field as well as for ducts with various aspect ratios in both vertical and horizontal magnetic fields. The paper is concluded with a summary and comparison with experimental results in §4. Our non-standard vector stream function/vorticity formulation is described in Appendix A.

## 2. Formulation of the problem

Consider a flow of an incompressible viscous electrically conducting liquid with density  $\rho$ , kinematic viscosity  $\nu$  and electrical conductivity  $\sigma$  driven by a constant gradient of pressure  $p$  applied along a straight duct of rectangular cross-section with half-width  $d$  and half-height  $h$  subject to a transverse homogeneous magnetic field  $\mathbf{B}$ . The walls of the duct are assumed to be perfectly electrically conducting and the field may be applied across either the width or the height of the duct.

The velocity distribution of the flow is governed by the Navier-Stokes equation

$$\partial_t \mathbf{v} + (\mathbf{v} \cdot \nabla) \mathbf{v} = -\rho^{-1} \nabla p + \nu \nabla^2 \mathbf{v} + \rho^{-1} \mathbf{f}, \quad (2.1)$$

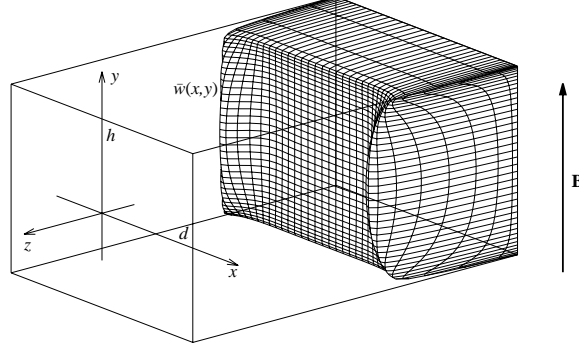


FIGURE 1. The base flow profile in a rectangular duct with perfectly conducting walls subject to a strong vertical magnetic field for  $Ha = 100$ .

where  $\mathbf{f} = \mathbf{j} \times \mathbf{B}$  is the electromagnetic body force involving the induced electric current  $\mathbf{j}$ , which is governed by the Ohm's law for a moving medium

$$\mathbf{j} = \sigma(\mathbf{E} + \mathbf{v} \times \mathbf{B}). \quad (2.2)$$

The flow is assumed to be sufficiently slow so that the induced magnetic field is negligible relative to the imposed one, which supposes the magnetic Reynolds number  $Rm = \mu_0 \sigma v_0 d \ll 1$ , where  $\mu_0$  is the permeability of vacuum and  $v_0$  is the characteristic velocity of the flow. In addition, we assume that the characteristic time of velocity variation is much longer than the magnetic diffusion time  $\tau_m = \mu_0 \sigma d^2$ , which allows us to use the quasi-stationary approximation leading to  $\mathbf{E} = -\nabla \phi$ , where  $\phi$  is the electrostatic potential (Roberts 1967). The velocity and current satisfy the mass and charge conservation  $\nabla \cdot \mathbf{v} = \nabla \cdot \mathbf{j} = 0$ . Applying the latter to the Ohm's law (2.2) yields

$$\nabla^2 \phi = \mathbf{B} \cdot \boldsymbol{\omega}, \quad (2.3)$$

where  $\boldsymbol{\omega} = \nabla \times \mathbf{v}$  is vorticity. At the duct walls  $S$ , the normal ( $n$ ) and tangential ( $\tau$ ) velocity components satisfy the impermeability and no-slip boundary conditions  $v_n|_S = 0$  and  $v_\tau|_S = 0$ . As the walls are perfectly conducting, the tangential electric current vanishes and Ohm's law (2.2) yields  $\phi|_S = \text{const}$ .

We employ the Cartesian coordinates with the origin set at the centre of the duct,  $x$ ,  $y$  and  $z$  axes directed along its width, height and length, respectively, as shown in figure 1, and the velocity defined as  $\mathbf{v} = (u, v, w)$ . The problem admits a purely rectilinear base flow with a single velocity component along the duct  $\bar{\mathbf{v}} = (0, 0, \bar{w}(x, y))$  which is shown in figure 1(a) for a strong vertical magnetic field.

In the following, all variables are non-dimensionalised by using the maximum velocity  $\bar{w}_0$  and the half-width of the duct  $d$  as the velocity and length scales, while the time, pressure, magnetic field and electrostatic potential are scaled by  $d^2/\nu$ ,  $\rho \bar{w}_0^2$ ,  $B = |\mathbf{B}|$  and  $\bar{w}_0 dB$ , respectively. The dimensionless parameters defining the problem are the Reynolds number  $Re = \bar{w}_0 d / \nu$ , the Hartmann number  $Ha = dB \sqrt{\sigma / (\rho \nu)}$  and the aspect ratio  $A = h/d$ . Note that we use the maximum rather than average velocity as the characteristic scale because the stability of this flow, as shown in the following, is determined by the former.

Linear stability of this flow is analysed using the same method as in our previous study (Priede, Aleksandrova & Molokov 2010). Since the method is based on a non-standard vector stream function formulation, it is briefly outlined in the Appendix.

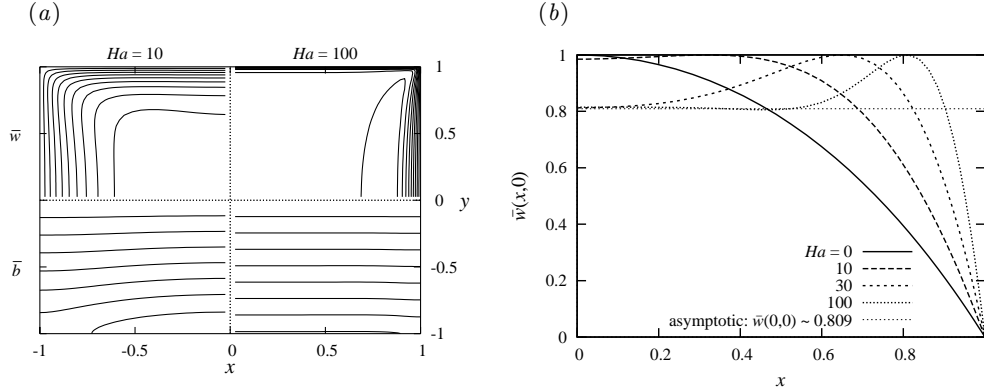


FIGURE 2. Isolines of the base flow ( $y > 0$ ) and electric current lines ( $y < 0$ ) for  $Ha = 10$  ( $x < 0$ ) and  $Ha = 100$  ( $x > 0$ ) shown in the respective quadrants of duct cross-section (a) and the base flow velocity profiles at  $y = 0$  for  $Ha = 0, 10, 30, 100$  (b) in a vertical magnetic field.

The problem was solved by a spectral collocation method on a Chebyshev-Lobatto grid with even number of points defined by  $2N_x + 2$  and  $2N_y + 2$  for the  $x$ - and  $y$ -directions, where  $N_{x,y} = 35 \cdots 60$  were used for various combinations of the control parameters to achieve accuracy of at least three significant figures. Owing to the double reflection symmetry of the base flow with respect to  $x = 0$  and  $y = 0$  planes, small-amplitude perturbations with different parities in  $x$  and  $y$  decouple from each other. This results in four mutually independent modes, which we classify as  $(o, o)$ ,  $(o, e)$ ,  $(e, o)$ , and  $(e, e)$  according to whether the  $x$  and  $y$  symmetry of  $\hat{\psi}_x$  is odd or even, respectively. Our classification of modes corresponds to the symmetries I, II, III, and IV used by Tatsumi & Yoshimura (1990) and Uhlmann & Nagata (2006). Thus, four independent problems of different symmetries are obtained in one quadrant of the duct cross-section with  $N_x \times N_y$  internal collocation points. The size of matrix for each eigenvalue problem is reduced by a factor of 16 in comparison to the original problem. Further details and the validation of the numerical method can be found in our previous paper (Priede, Aleksandrova & Molokov 2010).

### 3. Results

Flow in the presence of a vertical magnetic field induces a transverse current in the bulk of the duct which, as seen in the lower part of figure 2(a), almost directly connects to the perfectly conducting walls parallel to the magnetic field. However, a small part of the current diverts in the corner regions to connect through the Hartmann walls perpendicular to the magnetic field. This makes the density of the transverse current and so the resulting electromagnetic force, which opposes the constant driving pressure gradient, slightly lower at the parallel walls than in the core region. As a result, weak jets form along the parallel walls, where the flow becomes slightly faster than in the core of the duct. As seen in figure 2(a), the formation of jets starts with a velocity minimum appearing in the centre of the duct at  $Ha \approx 10$ . With the increase of the magnetic field, the velocity in the core becomes almost uniform, while the jets become confined in thin layers that develop along the walls parallel to the magnetic field and have a thickness decreasing as  $\sim Ha^{-1/2}$ . In a strong vertical magnetic field, asymptotic solution by Hunt (1965) yields the velocity maxima located in the mid-plane of the duct at the distance

$$\delta \approx 1.915(A/Ha)^{1/2} \quad (3.1)$$

from the parallel wall, while the ratio of this velocity to that of the core flow approaches a constant 0.809. The latter is seen in figure 2(b) to agree well with our numerical solution. An interesting feature of these jets is that the extra flow rate associated with the velocity over-shoot above the core velocity balances the flow rate deficit at the wall, where the velocity falls below that of the core (Williams 1962). Thus, the relative contribution of these jets to the flow rate is not  $\sim Ha^{-1/2}$ , as one would expect from simple scaling arguments, but a higher-order small quantity  $\sim Ha^{-3/2}$ , which is less than the flow rate correction due to the Hartmann layers  $\sim Ha^{-1}$ . It is confirmed also by our numerical solution, which yields the best fit of the flow rate for one quarter of a square duct

$$Q \approx 0.809 - 0.43Ha^{-1}, \quad (3.2)$$

where the leading-order contribution due to the core flow matches the asymptotic solution. Note that although the correction is  $\sim Ha^{-1}$ , its coefficient is not equal to that in the asymptotic solution by Hunt (1965). The difference is because the asymptotic solution is obtained for a fixed pressure gradient, whereas numerical solution is for a fixed maximum velocity, which has a  $O(Ha^{-1})$  higher-order correction. Thus, the maximum velocity taken as the reference one in this study, results in the same order correction in the core velocity and, thus, also in the flow rate. Our choice of the maximum velocity as the reference one is motivated by the following results, which show that the instability in this flow is associated with the jets at the parallel walls, which seem inherently unstable due to the inflection points in their velocity profiles. Our results can be rescaled to the average velocity using relation (3.2) which becomes sufficiently accurate for  $Ha \gtrsim 100$ .

We start with a square duct, in which the flow without the magnetic field is linearly stable (Tatsumi & Yoshimura 1990). The magnetic field renders the base flow linearly unstable at  $Ha \gtrsim 9.6$  with respect to a perturbation of symmetry type II. This perturbation is characterised by the vorticity component along the magnetic field being an odd function in the field direction and an even function spanwise. As shown in the following, the anti-symmetric distribution along the field results in a strong damping when the field strength is increased. The marginal Reynolds number at which the maximum growth rate for this mode turns zero ( $\Re[\lambda] = 0$ ) is plotted in figure 3(a) against the wavenumber for various Hartmann numbers. Besides the marginal Reynolds number, neutrally stable perturbations are characterised by their oscillation frequency  $\omega = \Im[\lambda]$  and the associated phase velocity  $-\omega/k$ . It is useful to consider the latter relative to the characteristic base flow velocity given by  $Re$ . This quantity defined as  $-\omega/(Rek)$  is subsequently referred to as the relative phase velocity and shown in figure 3(b) for mode II. Instability appears above the critical Reynolds number  $Re_c$ , which is defined by the global minimum on the neutral stability curve for the respective Hartmann number. With the increase of  $Ha$ , the critical Reynolds number for mode II in figure 3(a) first quickly drops to a minimum  $Re_c \approx 1.1 \times 10^4$  at  $Ha \approx 14$  and then starts to increase. In some ranges of the Hartmann number another minimum appears on the neutral stability curve, which may cause the critical mode to jump from the first to the second minimum as the latter becomes the global one. This switchover between global minima shows up as a jump in both the critical wavenumber and frequency, and as a break point in the dependence of the critical Reynolds number on the Hartmann number. Such a jump is noticeable in figure 5 at  $Ha \approx 48$ , where the instability switches from mode IIa to IIb.

However, this jump is of secondary importance because a mode of type I is seen in figure 5(a) to become more unstable than mode II at  $Ha \approx 10.6$ . Although mode I turns linearly unstable at a slightly higher Hartmann number than mode II, its critical Reynolds number decreases faster with the increase in the Hartmann number than that

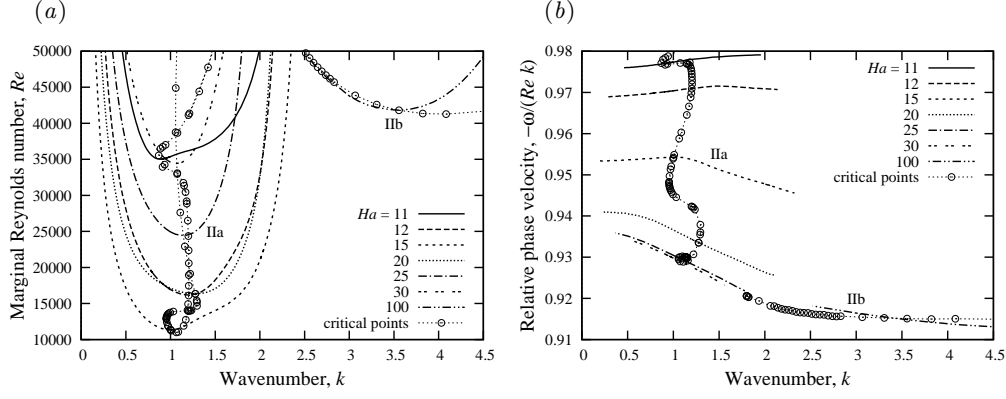


FIGURE 3. The marginal Reynolds number (a) and the relative phase velocity (b) versus the wavenumber for neutrally stable modes of type II in a square duct ( $A = 1$ ) subject to a vertical magnetic field at various Hartmann numbers.

for mode II. As seen from the neutral stability curves in figure 4(a,b), with the increase of the Hartmann number, the critical Reynolds number for mode I first quickly drops to a minimum  $Re_c \approx 2697$  at  $Ha \approx 17$  and then starts to raise. With the increase of  $Ha$  mode I is quickly approached from above by a mode of type III, which is seen in figure 5(a) to appear at  $Ha \approx 30$  and become practically indistinguishable from the former at  $Ha \gtrsim 80$ . There is also a mode of type IV appearing at  $Ha \approx 30$ , which in turn approaches mode II in a similar way as mode III approaches mode I. Modes III/IV differ from modes I/II by the opposite symmetry across the magnetic field. Namely, for modes III/IV, the vorticity component along the magnetic field is an odd function in the spanwise direction across the magnetic field, whereas it is an even function for modes I/II.

The most important feature of the instability seen in figure 5(a,b) is the critical Reynolds number and the wavenumber for each of two merged pairs of modes increasing in strong magnetic field as  $\sim Ha^{1/2}$ . The relative phase velocity shown in figure 5 tends to a constant  $\sim 0.911$  for both pairs of modes. This kind of variation implies that in a strong magnetic field the instability is determined by the internal length scale  $\delta \sim Ha^{-1/2}$ , which is the characteristic thickness of the jets developing along the walls parallel to the magnetic field. The base flow velocity correction of order  $\sim Ha^{-1}$ , which was discussed above, implies an  $O(Ha^{-1/2})$  correction to the critical Reynolds number. The best fit for modes I/III yields

$$Re_c(Ha; A = 1) \approx 642Ha^{1/2} + 8.9 \times 10^3 Ha^{-1/2}, \quad (3.3)$$

$$k_c(Ha; A = 1) \approx 0.477Ha^{1/2}, \quad (3.4)$$

which are seen in figure 5(a,b) to well approximate numerical results for mode I down to  $Ha \approx 30$ . Similarly, for modes II/IV, we find

$$Re_c(Ha; A = 1) \approx 2580Ha^{1/2} + 1.1 \times 10^5 Ha^{-1/2}, \quad (3.5)$$

$$k_c(Ha; A = 1) \approx 0.419Ha^{1/2}, \quad (3.6)$$

where the former is by nearly of a factor of four greater than (3.3).

The instability threshold being nearly the same for the modes of opposite spanwise symmetry in a sufficiently strong magnetic field implies that the perturbations developing in the jets at the opposite walls are effectively separated by the core region of the flow

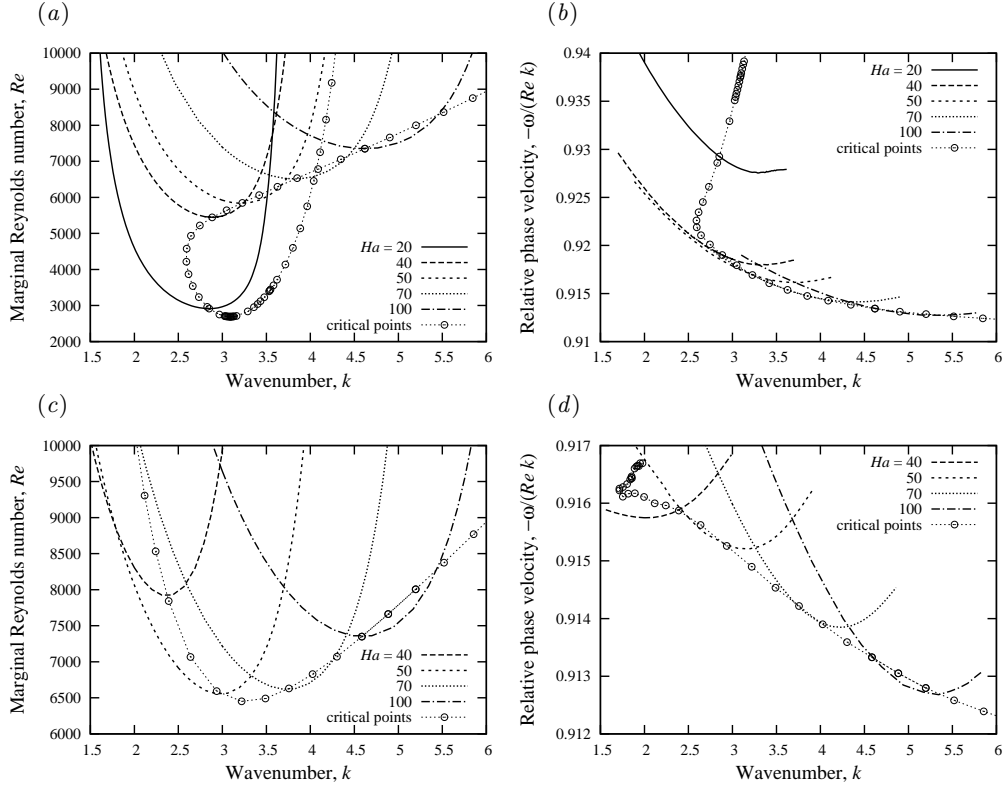


FIGURE 4. The marginal Reynolds number (a,c) and the relative phase velocity (b,d) versus the wavenumber for neutrally stable modes of type I (a,b) and type III (c,d).

and, thus, do not affect each other. This is confirmed by the patterns of the critical perturbations, which are plotted over the duct cross-section in figure 6 for a moderate ( $Ha = 15$ ) and a relatively strong ( $Ha = 100$ ) magnetic field. As shown in our previous paper (Priede, Aleksandrova & Molokov 2010), the flow perturbation can be represented by the complex amplitudes of the streamwise ( $z$ ) component of velocity ( $\hat{w}$ ) and that of stream function ( $\hat{\psi}_z$ ), whose isolines are plotted in the left ( $x < 0$ ) and the right ( $x > 0$ ) sides of the cross-section, respectively. The real and imaginary parts of perturbations plotted at the top and bottom halves of the cross-section show the instant patterns shifted in time or in the stream-wise direction by a quarter of period or wavelength, respectively. Although the real and imaginary parts of the complex amplitude distributions completely determine the evolution of perturbation over the harmonic oscillation cycle, these two quantities are not uniquely defined. The main ambiguity is due to the free choice of the initial time instant and the initial stream-wise coordinate. This ambiguity can be partly eliminated by choosing the phase of the complex velocity perturbation amplitude so that

$$\int_S \Re[\hat{v}]^2 ds = \int_S \Im[\hat{v}]^2 ds,$$

where the integrals are taken over the duct cross-section  $S$ . This condition defines the phase up to  $\pm\pi/2$ , which means swapping the real and imaginary parts. The perturbation amplitude remains defined up to a constant factor which is not important as the linear stability theory predicts only the pattern but not the amplitude of the critical perturbations.

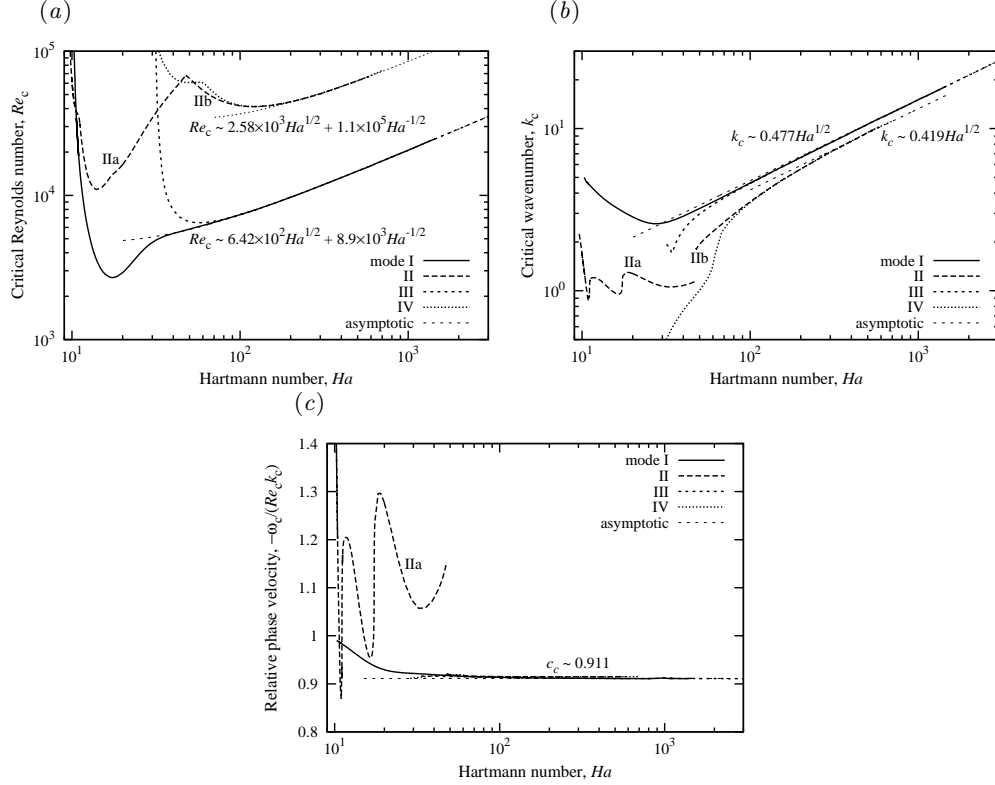


FIGURE 5. The critical Reynolds number (a), wavenumber (b) and relative phase velocity (c) against the Hartmann number.

Positive and negative values of  $\hat{w}$  are respectively associated with converging and diverging potential flow component in the cross-section plane. The isolines of  $\hat{\psi}_z$  correspond to the streamlines of the solenoidal flow component in that plane. The critical perturbations for modes I and II, which are shown in figures 6(a,b) and (d,e), respectively, differ by their vertical symmetry. Namely, the perturbation of  $\hat{w}$  and  $\hat{\psi}_z$  are respectively even and odd functions of  $y$  for mode I, whereas they are odd and even functions for mode II. Thus, the vortices for mode I rotate in opposite senses in the upper and lower parts of the cross-section, whereas for mode II there is one symmetric vortex spanning the whole height of the duct. For both of these modes, the pairs of vortices across the vertical mid-plane rotate in the same sense and, thus, represent two parts of a bigger vortex spanning over the whole width of the duct. At  $Ha = 15$ , slightly above the Hartmann number at which the flow turns linearly unstable, the critical perturbations are seen in figure 6(a,d) to be localised close to the duct centre, where the two velocity maxima discussed above first appear. In this case, the co-rotating vortices on the opposite sides of the duct, whose symmetric half is shown at  $x > 0$ , are clearly connected by the flow through the vertical mid-plane. However, this is no longer the case for a sufficiently strong magnetic field. As seen in figure in 6(b,e), at  $Ha = 100$  the critical perturbations for modes I and II are localised at the side walls. Moreover, these perturbations have nearly the same pattern as those for modes III and IV, which are shown in figure 6(c,f) for the same  $Ha$ . It means that in a strong enough magnetic field the perturbations at the opposite walls are effectively separated by a stagnant core flow and, thus, do not affect each other.



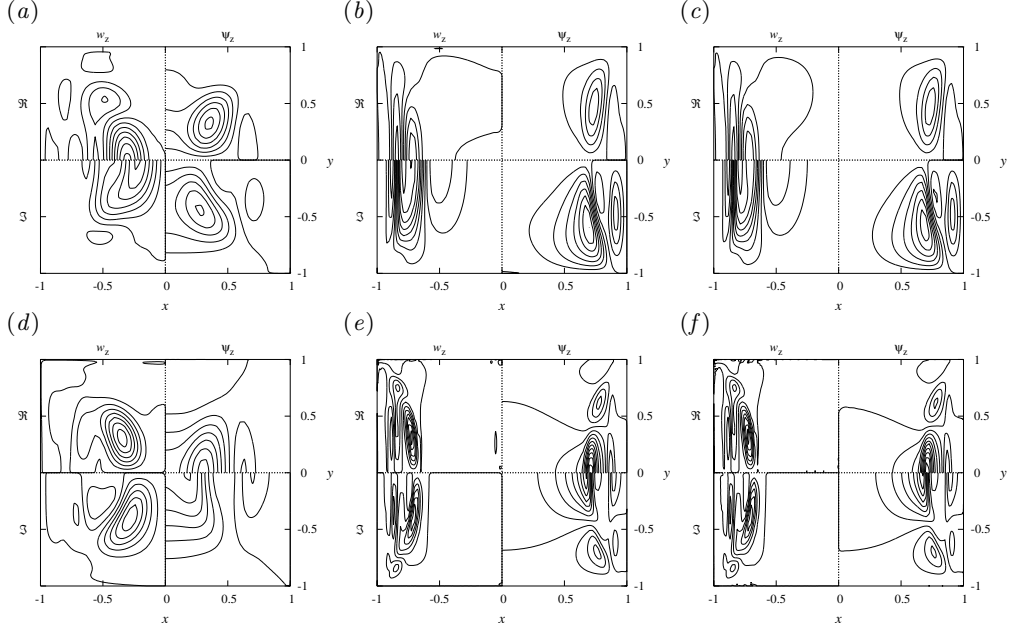


FIGURE 6. Amplitude distributions of the real ( $y > 0$ ) and imaginary ( $y < 0$ ) parts of  $\hat{w}$  ( $x < 0$ ) and  $\hat{\psi}_z$  ( $x > 0$ ) of the critical perturbations over one quadrant of duct cross-section for instability modes I (a,b), IIa (d,e), III(c) and IV(f) at  $Ha = 15$  (a,d) and  $Ha = 100$  (b,c,e,f).

This explains the merging of the instability thresholds for the modes with the opposite spanwise symmetries seen in figure 5.

In weaker magnetic fields or in narrower ducts across the magnetic field, which will be considered later, perturbations at the opposite walls can either enhance or suppress each other depending on their spanwise symmetry. The first is the case for the perturbations of type I/II, which, as discussed above, have co-rotating vortices at the opposite walls connected by a flow across the vertical mid-plane. These perturbations are more unstable than those of type II/IV with counter-rotating vortices at the opposite walls, which tend to suppress each other, especially in moderate magnetic fields or in sufficiently narrow ducts.

Besides the spatial amplitude distributions perturbations can be characterised quantitatively by their kinetic energy distribution, which can be represented in two different forms using either the velocity or vorticity/stream function components

$$E \propto \int_S |\hat{\mathbf{v}}|^2 ds = \int_S \Re[\hat{\boldsymbol{\omega}} \cdot \hat{\boldsymbol{\psi}}^*] ds,$$

where  $E$  is the kinetic energy of perturbation averaged over the wavelength and the asterisk denotes the complex conjugate (Priedit, Aleksandrova & Molokov 2010). At the moderate Hartmann number  $Ha = 15$  considered above, most of the kinetic energy, i.e. 60% and 66% for mode I and 88% and 53% for mode II, is carried by the  $z$ -component of velocity and by the  $y$ -component of vorticity, respectively. For mode I, next most energetic is the  $x$ -component of both velocity and vorticity, which contain respectively about 27% and 23% of the energy. For mode II, in this position are the  $y$  velocity and the  $x$  vorticity components, which contain respectively about 10% and 37% of the energy.

The energy distribution for the most unstable modes I and II becomes simpler in a strong magnetic field. For example, at  $Ha = 100$ , 86% of the energy for these modes is

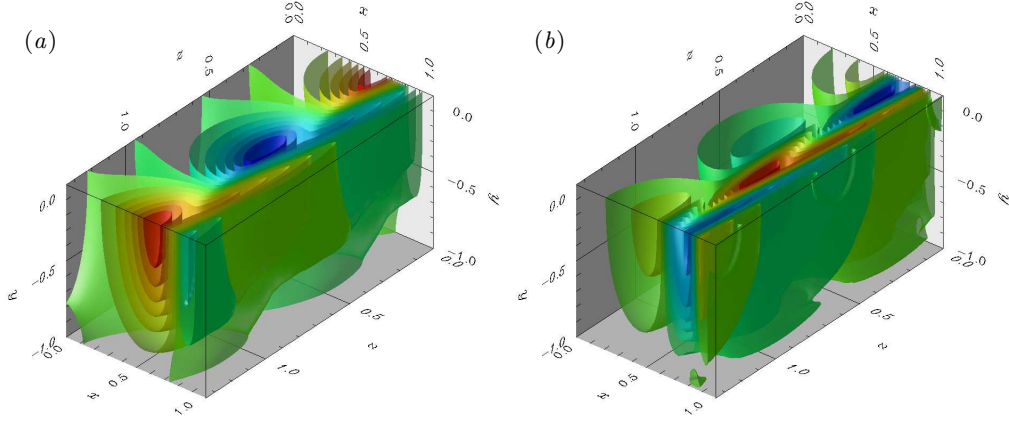


FIGURE 7. Isosurfaces of  $\hat{\psi}_y$  (a) and longitudinal velocity  $\hat{w}$  (b) perturbations over wavelength in one quadrant of the duct cross-section for instability mode I at  $Ha = 100$  in a vertical magnetic field.

concentrated in the  $y$ -component of vorticity, while the rest is distributed nearly equally between the two other vorticity components. This component of vorticity is associated with the circulation in the  $(x, z)$ -planes transverse to the magnetic field. The streamlines of this circulation are represented by the isolines of  $\psi_y$ , whose spatial distribution is shown in figure 7(a). Note that the distribution of  $\psi_y$  is very close to that of the electric potential  $\phi$  because the equations (A 6) and (A 5) governing both quantities are the same. Moreover,  $\psi_y$  and  $\phi$  satisfy the same boundary condition at the wall parallel to the magnetic field. Thus, both quantities differ only in the vicinity of the wall normal to the magnetic field, where they have different boundary conditions.

The transverse character of circulation for modes I and III is confirmed also by the kinetic energy distribution over the velocity components. Only about 9% of the energy is carried by the velocity component along the magnetic field, while 67% by the streamwise ( $z$ ) velocity perturbation, whose spatial distribution is shown in 7(b). The relatively low contribution of the spanwise ( $x$ ) velocity component, which carries the remaining 24% of the energy, is due to the relatively long wavelength of perturbation  $\lambda_c = 2\pi/k_c$ , which according to (3.4) is by approximately a factor of 7 larger than the thickness of the jet (3.1).

In a strong magnetic field, the energy distribution in modes II/IV is essentially different from that in modes I/II considered above. Namely, the latter two have only 5–6% of their energy in the spanwise ( $x$ ) velocity component, which implies a circulation constrained mainly to the  $(y, z)$ -planes parallel to the side walls. Similar to the previous two modes, 66% of the energy is carried by the streamwise velocity component. Although circulation mostly occurs in the  $(y, z)$ -planes, only 19% of the energy is contained the transverse ( $x$ ) vorticity/stream function component, while 56% are still contained in the vorticity/stream function component along the magnetic field. This scatter of energy between the vorticity components is due to the confinement of circulation in narrow layers parallel to the side walls. The confinement causes a strong variation of the velocity perturbation in the spanwise ( $x$ ) direction and, thus, produces a significant vorticity components tangential to the plane of circulation.

Finally, we consider the effect of the duct aspect ratio on the instability threshold of the two most unstable modes. In order to generalise the above results for square duct to arbitrary aspect ratios it is instructive to start with a horizontal magnetic field, which is

directed along the fixed dimension of the duct, i.e. the width in our case. In sufficiently strong horizontal magnetic field, the variation of the instability threshold with the aspect ratio turns out to be particularly simple and directly related to that of the square duct considered above. We shall use this fact and the similarity of horizontal and vertical magnetic field orientations to obtain more general relations for the latter orientation.

It is important to notice that the thickness of parallel layers  $\delta$  defined by (3.1), which is the characteristic length scale of the instability, varies not only with the Hartmann number but also with the aspect ratio  $A$ , which defines the size of the duct along the magnetic field. When the magnetic field is directed horizontally along the fixed dimension of the duct,  $\delta$  becomes independent of  $A$  and varies only with  $Ha$  as in the case of square duct. This simplification is our main motivation for considering first horizontal magnetic field.

On changing the magnetic field from vertical to horizontal, modes I/III swap with II/IV, which, thus, become the most unstable ones. For sufficiently large aspect ratios, the critical Reynolds number and the wavenumber are seen in figure 8(a,b) to be the same for both modes, which agree with the strong field asymptotics (3.3,3.4). As discussed above, this implies that the instabilities developing in the jets at the parallel walls are effectively separated by a stagnant core of the flow and, thus, do not affect each other. It changes at small aspect ratios, when the walls parallel to the magnetic field are sufficiently close to each other. Then the vortices at the opposite walls start to interact, which causes the thresholds for both modes to diverge. For mode IV, the vortices at the opposite walls counter-rotate and, thus, tend to suppress each other, which results in the stabilisation of the flow. It is the opposite for mode II, whose instability threshold first drops as the co-rotating vortices at the opposite walls start to enhance each other. However, with further reduction of the aspect ratio the critical Reynolds number attains a minimum and then starts to increase following that for mode IV. The raise of  $Re_c$  for mode II is associated with the increase of the critical wavenumber. This corresponds to the reduction of wavelength which is required for the vortices to fit between closely spaced parallel walls.

Now we turn to vertical magnetic field, which is oriented along the variable height of the duct. This slightly more complicated case can be reduced to the previous one by taking the height of the duct as the length scale and rotating the duct by 90 degrees. This is equivalent to the substitutions  $A' = 1/A$ ,  $Re' = ARe$ ,  $Ha' = AHa$ , and  $k' = Ak$ , where the parameters with primes correspond to the case of horizontal magnetic field considered above. Then we can use the result for horizontal magnetic field found above according to which the critical parameters in strong magnetic field approach those for a square duct given by (3.3,3.4). Substituting the primed parameters into (3.3,3.4) we obtain

$$Re_c(Ha; A) = A^{-1} Re_c(AHa; 1), \quad (3.7)$$

$$k_c(Ha; A) = A^{-1} k_c(AHa; 1), \quad (3.8)$$

which are seen in figure 8(c,d) to fit the numerical results well in the intermediate range of aspect ratios, where the thresholds for both most unstable modes I/III merge. In this range both the critical Reynolds number and wavenumber for a fixed  $Ha$  vary asymptotically with the aspect ratio as  $\sim A^{-1/2}$ . This variation, which is due to the increase of the jet width (3.1) as  $\sim A^{1/2}$ , breaks down at both small and large  $A$ . In the former limit, asymptotic relations (3.7,3.8) turn inapplicable because the effective Hartmann number  $AHa$  based on the height becomes too small for (3.3,3.4) to be valid. In the latter limit, the jets become so wide that the vortices at the opposite walls start to interact resulting

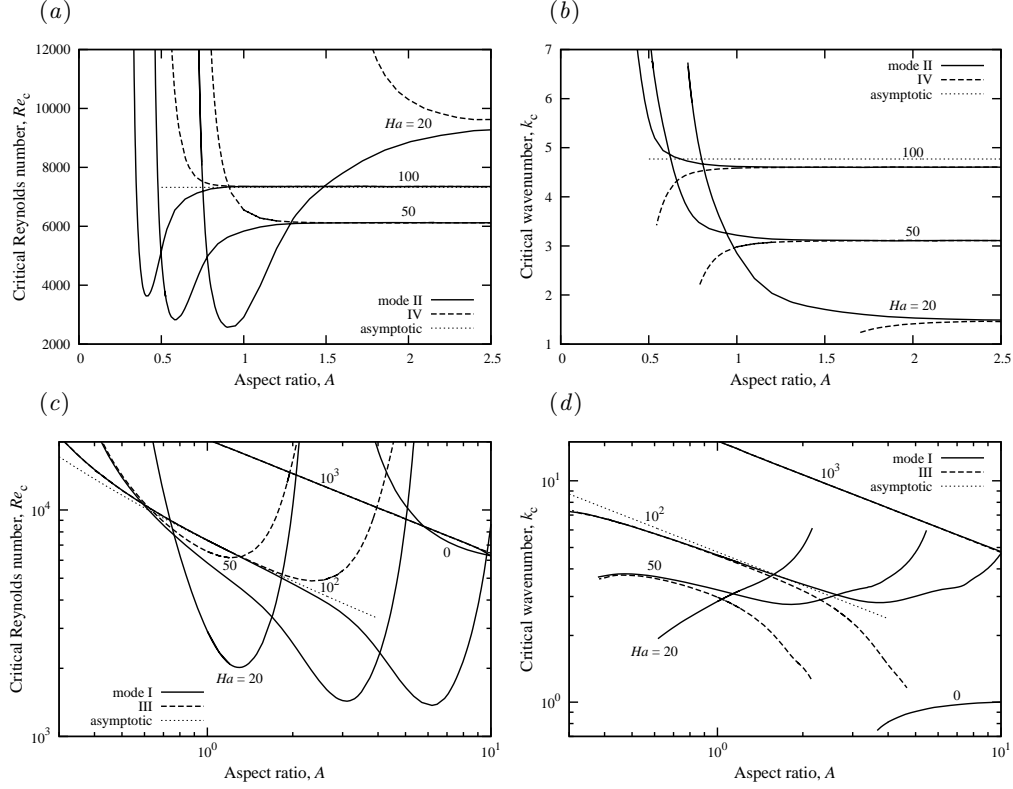


FIGURE 8. The critical Reynolds number (a,c) and the wavenumber (b,d) versus the aspect ratio for modes II/IV in a horizontal magnetic field (a,b) and for modes I/III in a vertical magnetic field (c,d) at various Hartmann numbers.

in the divergence of the instability thresholds and the eventual stabilisation described above for the case of horizontal magnetic field.

#### 4. Discussion and conclusions

We have presented numerical results concerning linear stability of a liquid metal flow in a rectangular duct with perfectly electrically conducting walls subject to a uniform transverse magnetic field. It was found that a linearly stable flow in a square duct turns unstable as a relatively weak magnetic field with the Hartmann number  $Ha \approx 9.6$  is applied. The instability is due to two weak jets, which first appear at the centre of the duct and then move to the walls parallel to the magnetic field as the field strength is increased. The instability follows the jets and in a sufficiently strong magnetic field becomes confined in the layers of characteristic thickness  $\delta \sim Ha^{-1/2}$  located at the parallel walls. The thickness  $\delta$  determines the characteristic length scale of the instability, which results in both the critical Reynolds and wave numbers scaling as  $\sim \delta^{-1}$ . Owing to the double reflection symmetry of the problem, perturbations with four different symmetry combinations along and across the magnetic field decouple from each other and, thus, are considered separately. The most unstable is a pair of perturbations with an even distribution of the vorticity along the magnetic field. These two modes represent strongly non-uniform vortices aligned with the magnetic field, which rotate either in the same or opposite directions across the magnetic field. The former enhance while the latter weaken

one another provided that the magnetic field is not too strong or the walls parallel to the field are not too far apart. In a strong magnetic field, when the vortices at the opposite walls are well separated from the core flow, the critical Reynolds number and wavenumbers for both of these instability modes are the same:  $Re_c \approx 642Ha^{1/2} + O(Ha^{-1/2})$  and  $k_c \approx 0.477Ha^{1/2}$ . The other pair of critical perturbations, which differs from the previous one by an odd distribution of vorticity along the magnetic field, is more stable with approximately four times higher critical Reynolds number.

The basic instability characteristics described above resemble those for the Hunt's flow, which has a similarly increasing, however a significantly lower, critical Reynolds number  $Re_c \sim 91Ha^{1/2}$  (Priede, Aleksandrova & Molokov 2010). The difference becomes substantial when the average rather than the maximum velocity is considered. Namely, the critical Reynolds number based on the average velocity for this flow increases in a strong magnetic field in the same way as  $\bar{Re}_c \approx 519Ha^{1/2}$ , whereas it tends to a constant  $\bar{Re}_c \approx 112$  for Hunt's flow. This asymptotically constant  $Re_c$  is due to a principally different velocity distribution in Hunt's flow with the jets of thickness  $\sim Ha^{-1/2}$  dominating the flow rate. Constant  $\bar{Re}_c \approx 313$  has been found by Ting *et al.* (1991) for the linear stability of the flow in a square duct with thin but relatively well-conducting walls in a strong transverse magnetic field. This flow represents an intermediate case in terms of the conductivity of parallel wall between the perfectly conducting one considered in this study and the insulating one for Hunt's flow. Although the leading-order velocity distribution considered by Ting *et al.* (1991) is nearly the same as that of Hunt's jet, there is one principal difference between two. Namely, in a duct with thin parallel walls of a moderate conductance ratio  $c = \sigma_w d_w / \sigma d$ , where  $\sigma_w$  and  $d_w$  are the electrical conductivity and the thickness of wall, satisfying  $Ha^{-1/2} \ll c \ll Ha^{1/2}$ , jets carry a volume flux of the same order of magnitude as that of the core flow, whereas the contribution of the latter is negligible in Hunt's flow. In a square duct with thin walls, in which the core flow in strong magnetic field carries 3/4 of the total volume flux (Walker 1981), the jet velocity is by a factor of about four lower than that for Hunt's flow at the same  $\bar{Re}$ . It means that jets are more unstable at wall of finite conductivity than in both limiting cases of insulating and perfectly conducting parallel walls.

The experiment best matching the model considered in this study has been carried out by Branover & Gelfgat (1968), who measured a flow of mercury at  $Re \approx 4 \times 10^4$  and  $Ha = 174$  in a rectangular copper duct with a relatively high wall conductance ratio, which was 20 and 10 for the Hartmann and the parallel walls, respectively. The magnetic field was applied transversely to the longest side of the duct with the aspect ratio of 1.5. First, the authors found a maximum velocity in jets exceeding the theoretical prediction for perfectly conducting duct by approximately 50%. At this Hartmann number, we find that 19% of the excess jet velocity may be due to the finite wall conductivity, when the latter is included in the numerical solution. Note that the effect of imperfectly conducting walls is not entirely determined by the relative conductance of the parallel layers  $cHa^{1/2}$  as it may appear from Hunt (1965) (see also Müller & Bühler 2001, p. 146). Namely,  $cHa^{1/2} \gg 1$  means only that the parallel walls cannot be treated as insulating ( $c \neq 0$ ). But it does not necessary mean that the walls may be assumed perfectly conducting ( $c = \infty$ ). As shown by Walker (1981), the latter approximation requires a much higher wall conductance ratio  $cHa^{-1/2} \gg 1$ . Thus, the effect of imperfectly conducting walls increases rather than decreases with the field strength, which results in the jet velocity relative to that of the core increasing with the field strength as  $\sim Ha^{1/2}/c$  (Walker 1981). However, the most significant deviation from the laminar flow solution by Hunt (1965) was the jet thickness, which was found by Branover & Gelfgat (1968) to be several times

greater than expected. Such a broadening of jets is likely to be due to the turbulence which is expected in the experiment at the Reynolds number significantly above the linear stability threshold  $\bar{Re}_c \approx 6850$  predicted by our analysis for this setup.

In conclusion, note that when the distance of the velocity maximum from the parallel wall (3.1) is taken as the length scale, (3.3) becomes  $Re_c^{\delta} \approx 1230$ . This small critical Reynolds number may be due to the inviscid nature of the instability caused by the inflection point of the base velocity profile. It also implies that the instability may be supercritical rather than subcritical as for typical shear flows. The supercritical character of instability may explain why it appears significantly above the linear stability threshold as recently reported by Kinet, Knaepen & Molokov (2009). They observed small-amplitude vortices in the jets at the parallel walls for  $2500 \leq \bar{Re} \leq 3700$  at  $Ha = 200$  in the numerical simulation of a flow in a rectangular duct with thin walls. These vortices were found to be subcritically unstable for  $3500 \leq \bar{Re} \leq 3700$ , which may correspond to the large amplitude instabilities observed in the experiments (Reed & Picologlou 1989; Burr *et al.* 2000). If the instability in perfectly conducting duct like that in ducts with thin walls of finite conductivity is supercritical, it is expected to appear above the absolute instability threshold which cannot be lower than that of the convective instability predicted by the classical linear stability analysis used in this study (Priede & Gerbeth 1997). The absolute instability threshold for these jet-type flows, at which small-amplitude self-sustained vortices are expected to appear, is not yet known.

S.A. is grateful to Leverhulme Trust for financial support of this work. The authors are indebted to the Faculty of Engineering and Computing of Coventry University for the opportunity to use its high performance computer cluster.

## Appendix A. Vector stream function/vorticity formulation

We use the vector stream function  $\boldsymbol{\psi}$ , which is introduced to satisfy the incompressibility constraint  $\nabla \cdot \mathbf{v} = 0$  for the flow perturbation by seeking the velocity distribution in the form  $\mathbf{v} = \nabla \times \boldsymbol{\psi}$ . Since the velocity is invariant upon adding the gradient of arbitrary function to  $\boldsymbol{\psi}$ , we can impose an additional constraint

$$\nabla \cdot \boldsymbol{\psi} = 0, \quad (\text{A } 1)$$

which is analogous to the Coulomb gauge for the magnetic vector potential  $\mathbf{A}$  (Jackson 1998). Similarly to the incompressibility constraint for  $\mathbf{v}$ , this gauge leaves only two independent components of  $\boldsymbol{\psi}$ .

The pressure gradient is eliminated by applying *curl* to (2.1). This yields two dimensionless equations for  $\boldsymbol{\psi}$  and  $\boldsymbol{\omega}$

$$\partial_t \boldsymbol{\omega} = \nabla^2 \boldsymbol{\omega} - Re \mathbf{g} + Ha^2 \mathbf{h}, \quad (\text{A } 2)$$

$$0 = \nabla^2 \boldsymbol{\psi} + \boldsymbol{\omega}, \quad (\text{A } 3)$$

where  $\mathbf{g} = \nabla \times (\mathbf{v} \cdot \nabla) \mathbf{v}$ , and  $\mathbf{h} = \nabla \times \mathbf{f}$  are the *curls* of the dimensionless convective inertial and electromagnetic forces, respectively.

The boundary conditions for  $\boldsymbol{\psi}$  and  $\boldsymbol{\omega}$  are obtained as follows. The impermeability condition applied integrally as  $\int_s \mathbf{v} \cdot d\mathbf{s} = \oint_l \boldsymbol{\psi} \cdot d\mathbf{l} = 0$  to an arbitrary area of wall  $s$  encircled by a contour  $l$  yields  $\psi_\tau|_s = 0$ . This boundary condition substituted into (A 1) results in  $\partial_n \psi_n|_s = 0$ . In addition, the no-slip condition applied integrally  $\oint_l \mathbf{v} \cdot d\mathbf{l} = \int_s \boldsymbol{\omega} \cdot d\mathbf{s}$  yields  $\omega_n|_s = 0$ .

Linear stability of the base flow  $\{\bar{\boldsymbol{\psi}}, \bar{\boldsymbol{\omega}}, \bar{\phi}\}(x, y)$  is analysed with respect to infinitesimal

disturbances in the form of harmonic waves travelling along the axis of the duct

$$\{\psi, \omega, \phi\}(\mathbf{r}, t) = \{\bar{\psi}, \bar{\omega}, \bar{\phi}\}(x, y) + \{\hat{\psi}, \hat{\omega}, \hat{\phi}\}(x, y)e^{\gamma t + \beta k z},$$

where  $k$  is a wavenumber and  $\gamma$  is, in general, a complex growth rate. This expression substituted into (A 2, A 3) results in

$$\gamma \hat{\omega} = \nabla_k^2 \hat{\omega} - Re \hat{g} + Ha^2 \hat{h}, \quad (\text{A } 4)$$

$$0 = \nabla_k^2 \hat{\psi} + \hat{\omega}, \quad (\text{A } 5)$$

$$0 = \nabla_k^2 \hat{\phi} - \hat{\omega}_{||}, \quad (\text{A } 6)$$

where  $\nabla_k \equiv \nabla_{\perp} + \beta k \mathbf{e}_z$ ;  $||$  and  $\perp$  respectively denote the components along and transverse to the magnetic field in the  $(x, y)$ -plane. Because of the solenoidality of  $\hat{\omega}$ , we need only the  $x$ - and  $y$ -components of (A 4), which contain  $\hat{h}_{\perp} = -\partial_{xy} \hat{\phi} - \partial_{||} \hat{w}$ ,  $\hat{h}_{||} = -\partial_{||}^2 \hat{\phi}$  and

$$\hat{g}_x = k^2 \hat{v} \bar{w} + \partial_{yy}(\hat{v} \bar{w}) + \partial_{xy}(\hat{u} \bar{w}) + \beta 2k \partial_y(\hat{w} \bar{w}), \quad (\text{A } 7)$$

$$\hat{g}_y = -k^2 \hat{u} \bar{w} - \partial_{xx}(\hat{u} \bar{w}) - \partial_{xy}(\hat{v} \bar{w}) - \beta 2k \partial_x(\hat{w} \bar{w}), \quad (\text{A } 8)$$

where

$$\hat{u} = \beta k^{-1}(\partial_{yy} \hat{\psi}_y - k^2 \hat{\psi}_y + \partial_{xy} \hat{\psi}_x),$$

$$\hat{v} = -\beta k^{-1}(\partial_{xx} \hat{\psi}_x - k^2 \hat{\psi}_x + \partial_{xy} \hat{\psi}_y),$$

$$\hat{w} = \partial_x \hat{\psi}_y - \partial_y \hat{\psi}_x.$$

The relevant boundary conditions are

$$\hat{\phi} = \hat{\psi}_y = \partial_x \hat{\psi}_x = \partial_x \hat{\psi}_y - \partial_y \hat{\psi}_x = \hat{\omega}_x = 0 \text{ at } x = \pm 1, \quad (\text{A } 9)$$

$$\hat{\phi} = \hat{\psi}_x = \partial_y \hat{\psi}_y = \partial_x \hat{\psi}_y - \partial_y \hat{\psi}_x = \hat{\omega}_y = 0 \text{ at } y = \pm A. \quad (\text{A } 10)$$

## REFERENCES

- Braginskii, S. I. (1960) Magnetohydrodynamics of weakly conducting liquids. *Sov. Phys. JETP* **107**, 1005–1014.
- Branover, G. G. & Gelfgat, Yu. M. 1968 *Fluid Dynamics* **1**, 79.
- Brouillette, E. C. & Lykoudis, P. S. 1967 Magneto-fluid-mechanic channel flow. I. Experiment. *Phys. Fluids* **10**, 995–1001.
- Bühler, L. 2007 Liquid metal magnetohydrodynamics for fusion blankets. In: *Molokov, S., Moreau, R., Moffatt, H.K. (eds.), Magnetohydrodynamics: Historical Evolution and Trends*. Springer, pp. 171–194.
- Burr, U., Barleon, L., Müller, U. & Tsinober, A. 2000 Turbulent transport of momentum and heat in magnetohydrodynamic rectangular duct flow with strong sidewall jets. *J. Fluid Mech.* **406**, 247–279.
- Chang, C. C. & Lundgren, T. S. 1961 Duct flow in magnetohydrodynamics. *ZAMP* **12**, 100–114.
- Drazin P.G. & Reid W. H. 1981 *Hydrodynamic Stability*, Cambridge, §31.6.
- Hocking, L. M. (1975) Non-linear stability of the asymptotic suction velocity profile. *Quart. J. Mech. Appl. Math.* **28**, 341–353.
- Hunt, J. C. R. 1965 Magnetohydrodynamic flow in rectangular ducts. *J. Fluid Mech.* **21**, 577–590.
- Jackson, J. D. 1998 *Classical Electrodynamics*, Wiley, §6.3.
- Kakutani T. 1964 The hydrodynamic stability of the modified plane Couette flow in the presence of a transverse magnetic field. *J. Phys. Soc. Japan* **19**, 1041–1057.
- Kinet, M., Knaepen, B. & Molokov, S. 2009 Instabilities and transition in magnetohydrodynamic flows in ducts with electrically conducting walls. *Phys Rev Lett.* **103**, 154501.
- Lifshits, A. M. & Shtern, V. N. 1979 Monoharmonic analysis of the nonlinear stability of Hartmann flow. *Magnetohydrodynamics* **15**, 243–248.

- Lock R. C. 1955 The stability of the flow of an electrically conducting fluid between parallel planes under a transverse magnetic field. *Proc. Roy. Soc. Lond.(A)* **233**, 105–125.
- Moresco, P. & Alboussière, T. 2003 Weakly nonlinear stability of Hartmann boundary layers, *Eur. J. Mech. B Fluids* **22**, 345–353.
- Moresco, P. & Alboussière, T. 2004 Experimental study of the instability of the Hartmann layer. *J. Fluid Mech.* **504**, 167–181.
- Müller, U. & Bühler, L. 2001 *Magnetohydrodynamics in Channels and Containers*. Springer.
- Murgatroyd, W. 1953 Experiments in magnetohydrodynamic channel flow. *Phil. Mag.* **44**, 1348–1354.
- Pothérat, A. 2007 Quasi two-dimensional perturbations in duct flows with a transverse magnetic field. *Phys. Fluids* **19**, 74104.
- Priede, J. & Gerbeth, G. 1997 Convective, absolute and global instabilities of thermocapillary–buoyancy convection in extended layers. *Phys. Rev. E* **56**, 4187–4199.
- Priede, J., Aleksandrova, S. & Molokov, S. 2010 Linear stability of Hunt’s flow. *J. Fluid Mech.* **649**, 115–134.
- Reed, C. B. & Picologlou, B. F., 1989 Side wall flow instabilities in liquid metal MHD flows under blanket relevant conditions. *Fusion Tech.* **15**, 705–715.
- Roberts, P. H. 1967 *An Introduction to Magnetohydrodynamics*, Longmans, §2.1.
- Shatrov, V. & Gerbeth, G. 2010 Marginal turbulent magnetohydrodynamic flow in a square duct. *Phys. Fluids* **22**, 084101–9.
- Shercliff, J. A. 1953 Steady motion of conducting fluids in pipes under transverse magnetic fields. *Proc. Cambr. Philos. Soc.* **49**, 136–144.
- Tatsumi, T. & Yoshimura, T. 1990 Stability of the laminar flow in a rectangular duct. *J. Fluid Mech.* **212**, 437–449.
- Ting, A. L., Walker, J. S., Moon, T. J., Reed, C. B. & Picologlou, B. F. 1991 Linear stability analysis for high-velocity boundary layers in liquid–metal magnetohydrodynamic flows. *Int. J. Engng. Sci.* **29**, 939–948.
- Uflyand, Ya. S. 1961 Flow stability of a conducting fluid in a rectangular channel in a transverse magnetic field. *Soviet Physics: Technical Physics* **30**, 1191–1193.
- Uhlmann, M. & Nagata, M. 2006 Linear stability of flow in an internally heated rectangular duct. *J. Fluid Mech.* **551**, 387–404.
- Williams W. E 1962 Magnetohydrodynamic flow in a rectangular tube at high Hartmann numbers. *J. Fluid Mech.* **16**, 262–268.
- Walker, J. S. 1981 Magnetohydrodynamic flows in rectangular ducts with thin conducting walls. *J. de Mécanique* **20**, 79–112.